Nat Hazards
DOI 10.1007/s11069-011-9726-7

ORIGINAL PAPER

Geomagnetic anomaly at Lunping before the 1999 Chi-Chi earthquake (M_w = 7.6) in Taiwan

Kuang-Jung Chen · Bonbbon Chiu · Jee-Shiang Wang · Cheng-Yu Lee · Cheng-Horng Lin · Kevin Chao

Received: 18 March 2009 / Accepted: 11 January 2011

Abstract A strong earthquake with a magnitude of 7.6 ($M_L = 7.3$) occurred on September 21, 1999, in central Taiwan. In order to discern any potential precursors before this earthquake, geomagnetic data at Lunping (LNP), Taiwan, Geomagnetic Observatory situated 100 km from the epicenter are examined using two methods, i.e., the traditional induction arrows and complex demodulation. Our results show that the remarkable temporal variation of real induction arrows appear to be strong prior to the great earthquake over the previous 24 months. After the great earthquake, the magnitudes of induction arrows decreased to the normal (mean of 8 years) levels. In other words, the direction of real induction arrows of the periods 30 and 20 min rotated 85° and 40° anticlockwise, respectively, before the Chi-Chi earthquake and returned to mean direction of last 10 years after the earthquake. A horizontal source field model using the finite difference method for 3-D shows that the variation of the real induction arrows might be ascribed to the conductivity variation body, which is 5 km buried at the epicenter area of the Chi-Chi earthquake, changing its conductivity from 0.002S/m to 0.06 S/m. The ratios of modulus (demodulated by using the complex demodulation method) over a period 12, and 8 h relative to the period of 24 h reveal a remarkable change that appeared 4–5 months prior to this strong earthquake. They increased gradually from the beginning of 1999 to August 1999 and decreased again to a (8 years) mean level after the strong earthquake occurrence. We consider that the variation of the induction arrow might be ascribed to the conductivity anomaly, which is buried 5 km at the south-east side of LNP with a conductivity change of 0.06 S/m. We propose that this elevation might be related to the preparation process of the great earthquake.

K.-J. Chen (✉) · B. Chiu · J.-S. Wang · C.-Y. Lee
Department of Earth Sciences, National Taiwan Normal University, Taipei 116, Taiwan
e-mail: kjchen@ntnu.edu.tw

C.-H. Lin
Institute of Earth Sciences, Academia Sinica, Taipei, Taiwan

K. Chao
School of Earth and Atmospheric Sciences, Georgia Institute of Technology, Atlanta, GA 30332, USA

Published online: 30 January 2011

Keywords Induction arrow · Geomagnetic field · Chi-Chi earthquake

1 Introduction

During the seismogenic period of earthquakes, the conductivity properties underground may change with time causing a subsequent variation in magnetic induction. Such an effect is called the "seismo-electromagnetic-induction effect". In studies of geomagnetic induction, it is common to search for empirical relationships between different components that are observed independently in time. "Parkinson's relation" was introduced to explain this phenomenon, as it expresses a linear relationship first observed by Parkinson (1959) and Rikitake and Yokoyama (1955). In earthquake precursor studies, the time change in the direction of a geomagnetic induction vector is available for monitoring the possible conductivity change in the crust or upper mantle. There are two types of techniques to study the "induction effect". The first method is to measure the variations of transfer functions with time. This method sometimes uses only single station data, or sometimes inter station data are considered. Yanagihara (1972) and Miyakoshi (1975) calculated the temporal variation in geomagnetic transfer functions that are considered to be associated with the 1923 Kanto earthquake with a magnitude of 7.8 and the Tashkent earthquake with a magnitude of 5.0. Later, similar and more precise work concerned with other earthquake occurrences can be found in the literature of Yanagihara and Nagano (1976); Rikitake (1966); Honkura (1979); Sano (1980); Shiraki (1980); (Chen 1981a, b); Gong (1985); Fujita (1990) and Chen and Fung (1993). Precursors of anomalous electromagnetic activity prior to earthquakes have been reported in many papers (e.g., Beamish 1982; Rikitake, 1987a, b, 1997; Fraser-Smith et al., 1990; Yoshino et al. 1993; Oike and Murakami 1993; Fujinawa and Takanashi 1994; Pulinets 1998; Liu et al. 2000; Zeng et al. 2001; 2002; Nagao et al. 2002; Yen et al., 2004). During the last twenty years, many of the results regarding the temporal variation of geomagnetic variation related to earthquake have been reported in many different places globally [Yanagihara 1972; Yanagihara and Nagano 1976; Xu et al. 1978; Rikitake 1966; Niblett and Honkura 1980; Shiraki 1980; Gong 1985; Chen and Fung 1985; Fujita 1990; Fujiwara and Toh 1996]. Some of the papers (Chen 1981a, b; Chen and Fung 1990; Chen and Fung 1993; Chen et al. 2006) indicated quite a remarkable secular change in transfer function at the Lunping Observatory in Taiwan and suggested that it might be associated with a large seismic event. They also found quite rapid changes in transfer functions at this observatory over a period of a few weeks before and after some major seismic events.

The second type of observational technique is to measure the time variations of the amplitude ratios of two different frequency components. Spectral analysis is the most popular way to realize the relative energy distribution for each frequency component without knowing the actual time function of these individual frequency bands. The complex demodulation (CD) method provides the best way to decompose the observed data consisting of different frequency components to their all single components. The CD method is especially suited to obtain filtering results, as is with most methods, but can also obtain the amplitude of the filtered component unlike other methods. The relative energy response for single frequency varies with time can be retrieved by the CD method. The time function of amplitude of each single frequency component from the start to the end of the observed data can be well noted by this method. Using this method, we will derive the time function of particular and significant frequency components of total intensity

geomagnetic data in Lunping to search for possible precursors before the occurrence of a great earthquake.

Taiwan is located in conductivity anomaly region (Chen et al. 2001; Chen and Chen 1998; Hsu et al. 1998; Hsu et al. 2008; Yen et al. 2009) in the western Pacific Ocean and lies atop a well-known seismically active region. A great earthquake of magnitude 7.3 ($M_L = 7.3$, $M_w = 7.6$) occurred on September 21, 1999, near the small town of Chi-Chi in Nantou County in central Taiwan (Shin 2000). The epicenter of the main shock was located at 120.82°E, 23.85°N with a focal depth of 8.0 km. The focal mechanism was a thrust type with a strike of 5°, dip of 34°, and rake of 65° (Chang et al. 2000). The distribution of aftershocks extends about 40 by 100 squr km horizontally and from 15 to 25 km in depth (Shin 2000). Most of the aftershocks occurred on the eastern side of the Chelungpu fault because the fault is an east-dipping thrust fault (Fig. 1). The daily number of earthquakes decreased monotonically in the aftershock stage and by 1 or 2 months after the main shock was at nearly the same level as before the main shock. Therefore, as a feasibility study, the temporal variation in short-period magnetic variations at Lunping Observatory (121°10′E, 25°00′N, in Taiwan, see Fig. 1) is derived by induction arrows and the modulus ratios of particular periods to search for a possible precursor to this great earthquake.

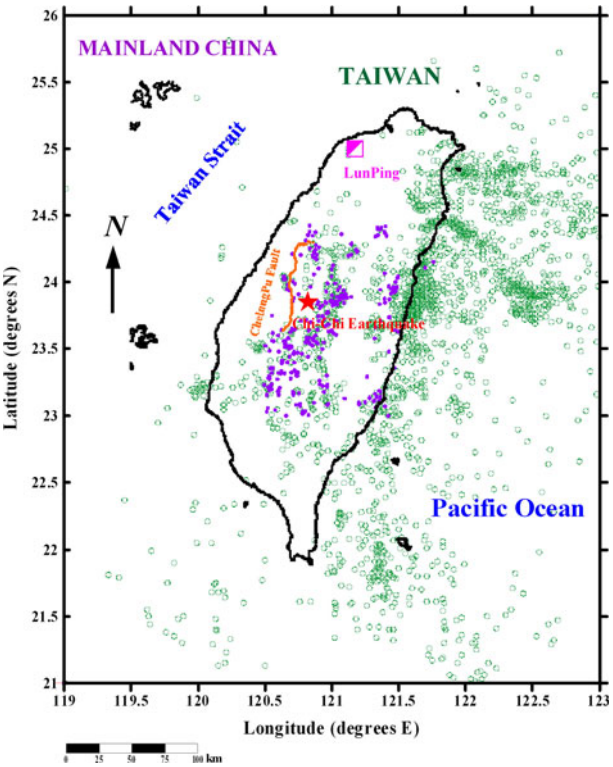

Fig. 1 The location of the Lunping Magnetic Observatory. Green hollow circles denote the events with magnitude M_L >3.5 occurring in Taiwan area in the study period. The epicenter of the major event of the 1999 Chi-Chi earthquake (*red star*), aftershocks (*purple solids*), and its coseismic fault, the ChelungPu fault, is also shown

2 Induction arrows

An electromotive force within the earth will occur when the geomagnetic field changes. This electromotance gives rise to eddy currents since the Earth has a finite conductivity. At non-polar stations, the directions of the different vectors for intervals less than an hour generally show a tendency to occur on or near a plane. This plane is called the "preferred plane" (Parkinson 1959). Induction arrows were developed following this assumption and were used in geomagnetic induction studies to summarize anomalous magnetic fluctuations and to indicate regions of high electrical conductivity. Such arrows are now regularly computed as real and imaginary vectors.

The short-period magnetic data of the Lunping Magnetic Observatory for the period of 1993–2000 were analyzed. Since 1965, the tri-axial fluxgate magnetometers at this station have been used to collect data at 1-min intervals. These instruments have a temperature of dependence of 0.2 nT/°C for the sensor and 0.1 nT/°C for the control unit, with a stability of 0.1 nT/day and resolution of 0.1 nT. The sensor is mounted on gimbals so that Z is aligned with the vertical direction by gravity, and the sensor case is buried to reduce the effects of ambient temperature changes. The temperature effects of each potentiometer is −0.302, −0.973, and −0.096 nT/°C for the Y, X, and Z component resistors, respectively. Timing accuracy is within 3 s [Huang 1990].

The induction arrows are calculated by the method derived by Everett and Hyndman (1967). In the first step, transfer functions were obtained by the least-squares fitting method. The concept of transfer functions comes from an empirical relation

$$\Delta Z = A\Delta H + B\Delta D \tag{1}$$

where ΔD is the variation of magnetic declination, ΔH and ΔZ are the variations of horizontal and vertical components, respectively, and the coefficients A and B are called transfer functions, which are complex and frequency dependent. The data analysis of the transfer functions is similar to the paper of Chen et al. (2006). Therefore, the induction arrow can be divided into two vectors: the real induction arrow ($R_{\max}$) and the imaginary induction arrow ($R_{\min}$), whose components are the real parts of A and B and the imaginary parts of A and B, respectively. An equivalent description is an ellipse with real induction and imaginary induction arrow having orientations θ_m, $\theta_m + 90^{\circ}$ and phase ϕ_m, $\phi_m + 90^{\circ}$. The ellipse can be obtained by maximizing $R^2 = (A\cos\theta + B\sin\theta)\left(\overline{A}\cos\theta + \overline{B}\sin\theta\right)$ with respect to θ, and solving for θ_m, $R_{\max}$, $R_{\min}$, and ϕ_m. The expression as an ellipse can be useful when considering a simple conductivity anomaly. For example, if a zone of high conductivity occurs near the recording station, the major axis will point at the center of the zone. If the zone is symmetric on either side of its center, then the minor axis of the ellipse will be zero. In this instance, however, the major part of the transfer function is real which will be seen to show much more coast effect than do the imaginary parts.

Daily means of the transfer functions relative to frequencies were carried out over 8 years from 1993 to 2000, regardless of the degree of magnetic disturbance. Fig. 2 shows the time–frequency plot of transfer functions for frequency range between 0.1 and 10 cycles/hour. As clearly seen in Fig. 2, transfer functions change smoothly over the frequency range between 0.1 and 10 cycles/hour, but they are oscillatory at a high-frequency range. Three significant frequencies ranges at 1.98–2.02, 2.82–2.90, and 4.10–4.18 cycles/hour (period ranges in 29.7–30.3 (*P1*), 20.7–21.3 (*P2*), and 14.4–14.6 min (*P3*)) can be found in real part (*Au* and *Bu*) over the whole study period. In order to verify these particular frequencies, we introduced the temporal variation in transfer

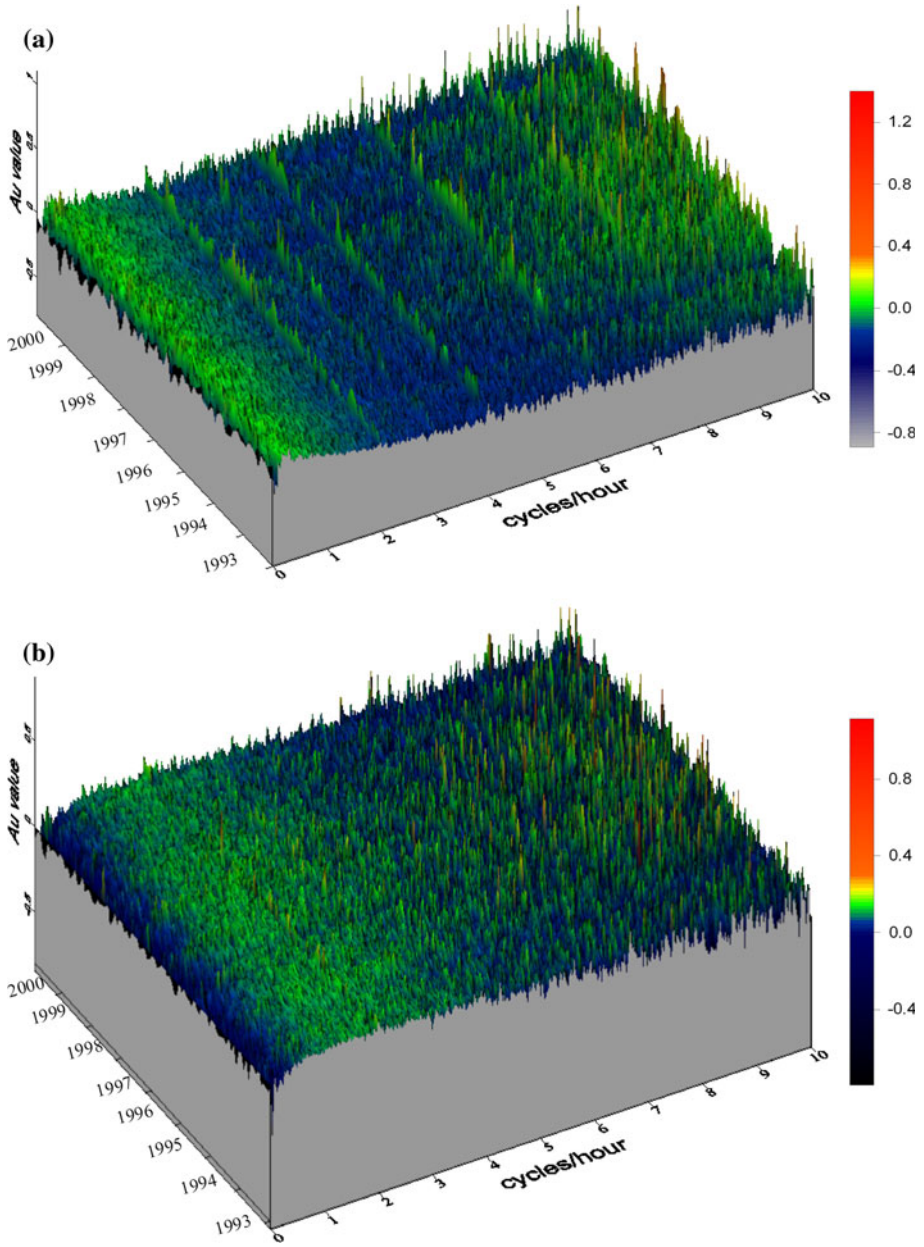

Fig. 2 Transfer functions **a** *Au,* **b** *Av*, **c** *Bu*, and **d** *Bv* calculated for frequency range between 0.1 and 10 cycles/hour from the Lunping Magnetic Observatory during the period 1993–2000

functions observed at three geomagnetic observatories ASP (Alice Springs, Australia, 133° 53′E, 23°46′S), WNG (Wingst, Germany, 90°4′E, 53°45′N), and YKC (Yellow Knife, Canada, 245°30′E, 62°30′N) in "seismicity quiet areas" (earthquakes occurring with magnitude greater than M_L 3.0, within 200 km from these stations are listed in Table 1).

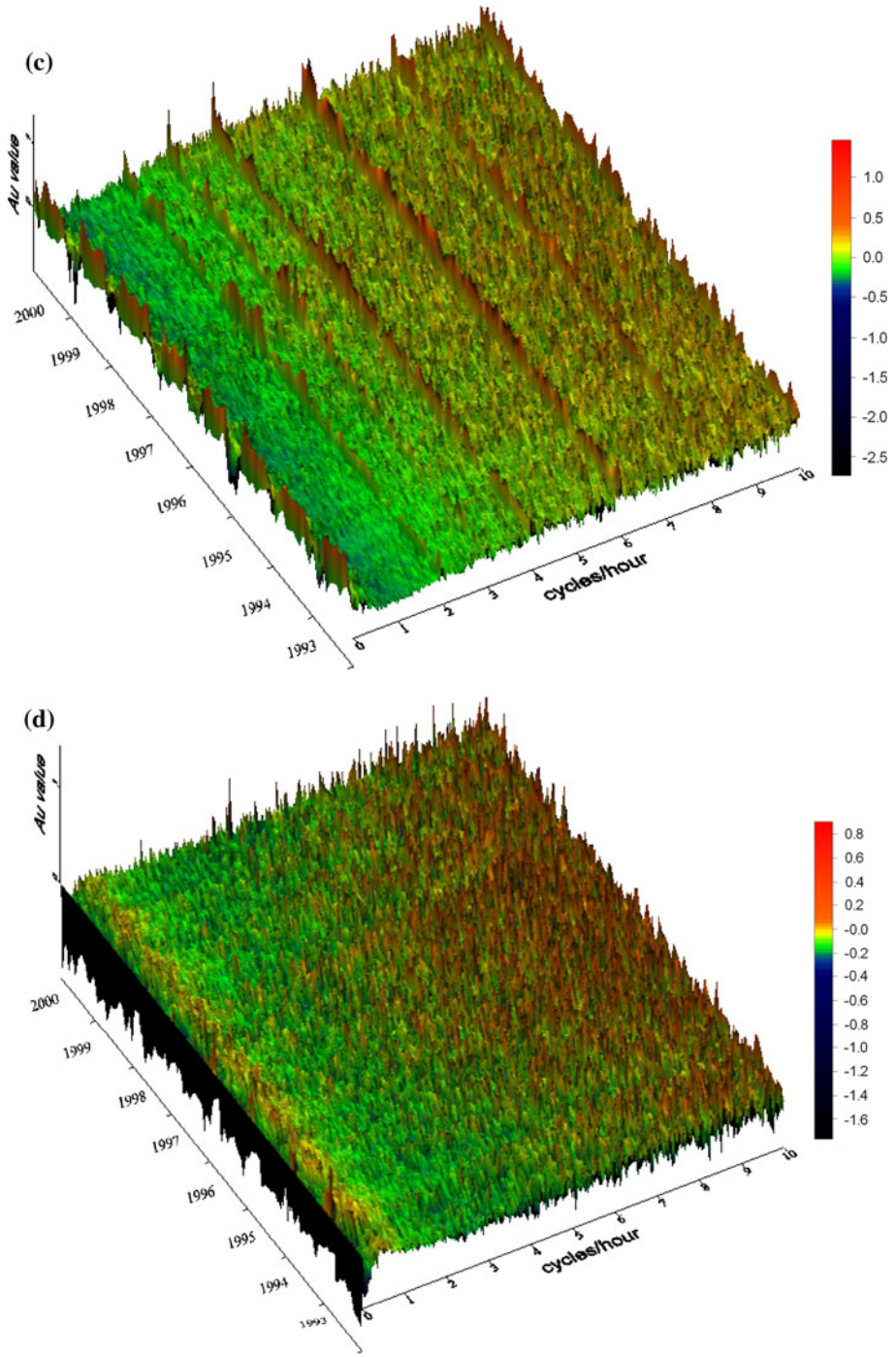

Fig. 2 continued

Table 1 The earthquakes occurred within 200 km from stations ASP, WNG, and YKC during 1988–2001 with magnitude $M_L \geq 3.0$ (located by incorporated research institutions for seismology (IRIS))

Relative to stations	Date	M_L
ASP	1991/04/18 04:51:05	3.1
ASP	1991/11/28 04:18:59	3.1
ASP	1996/07/19 14:14:55	3.5
ASP	1998/06/16 15:12:58	3.2
WNG	1997/11/19 05:15:38	4.3
WNG	1998/12/26 08:32:09	3.4
YKC	1990/03/30 07:53:54	3.5

Figure 3 shows the month-to-month variations of *Au* in the interval of 1992–2000. We can easily find that all the three stations in "seismically quiet" areas did not show any significant period. In other words, the frequency ranges *P1*, *P2*, and *P3* exist at Lunping station are extremely particular and might be caused locally.

The seasonal effect in the Taiwan area has been found by Chen et al. (2006). After removing the seasonal effect, using the same method, the monthly averages of induction arrows of three significant frequency ranges in 1.98–2.02, 2.82–2.90, and 4.10–4.18 cycles/hour (period ranges in 29.7–30.3 (*P1*), 20.7–21.3 (*P2*), and 14.4–14.6 min (*P3*)) are obtained. Figure 4 shows the time dependence of real Pakinson arrows (R_{max}) and imaginary arrows (R_{min}). The measured real induction arrows at Lunping changed remarkably with a bulge (*A1*) in August for *P1* and *P3,* and in October 1997 for *P2* about 24 and 22 months prior the Chi-Chi earthquake, respectively. Since the induction vector is always driven by the magnetic anomaly body, the dimension of the body owns its relative frequency band. The time lag between these two periods may be caused by the induction difference owing to different frequency bands. Other bulges can also be found in the variation of the imaginary arrow for *P1* and *P2* in May 1998 about 18 months prior the Chi-Chi earthquake. Figure 5 shows the time-dependent changes in the direction of real induction arrows (θ_m). The secular average direction of real induction arrows (θ_m) of these characteristic period ranges in *P1*, *P2*, and *P3* are N12°E, N16°E, and N0.2°E. All of these temporal variations are almost flat during the study period except two significant bulges (*B1* in September 1998 for *P1*, and *B2* in January 1999 for *P2*) prior the Chi-Chi earthquake. In other words, the direction of real induction arrows at *P1* and *P2* rotated 85° and 40° anticlockwise, respectively, before the Chi-Chi earthquake and return to its normal (near the 8 years mean value) direction after the earthquake. Based on the model calculation by Chen and Fung (1989), it implied that there is a sensitive resistivity structure anomaly south of the Lunping station. We consider that the variation of the real induction arrows might be ascribed to the elevation on the top level of a conductivity anomaly, which is buried deeply on the southern side of the Lunping Observatory. We propose that this elevation might be related to the preparation process of the Chi-Chi earthquake Fig. 6.

3 Modulus of the total intensity

The complex demodulation method is one of the Fourier-based time series analyses. Banks (1975) first introduced the application of the CD method into the field of geophysics. Chen et al. (2007) using the same method obtained several significant correlations between seismicity and the changes in magnetic modulus. The complex demodulation method provides one of the ways to decompose the observed data consisting of different frequency

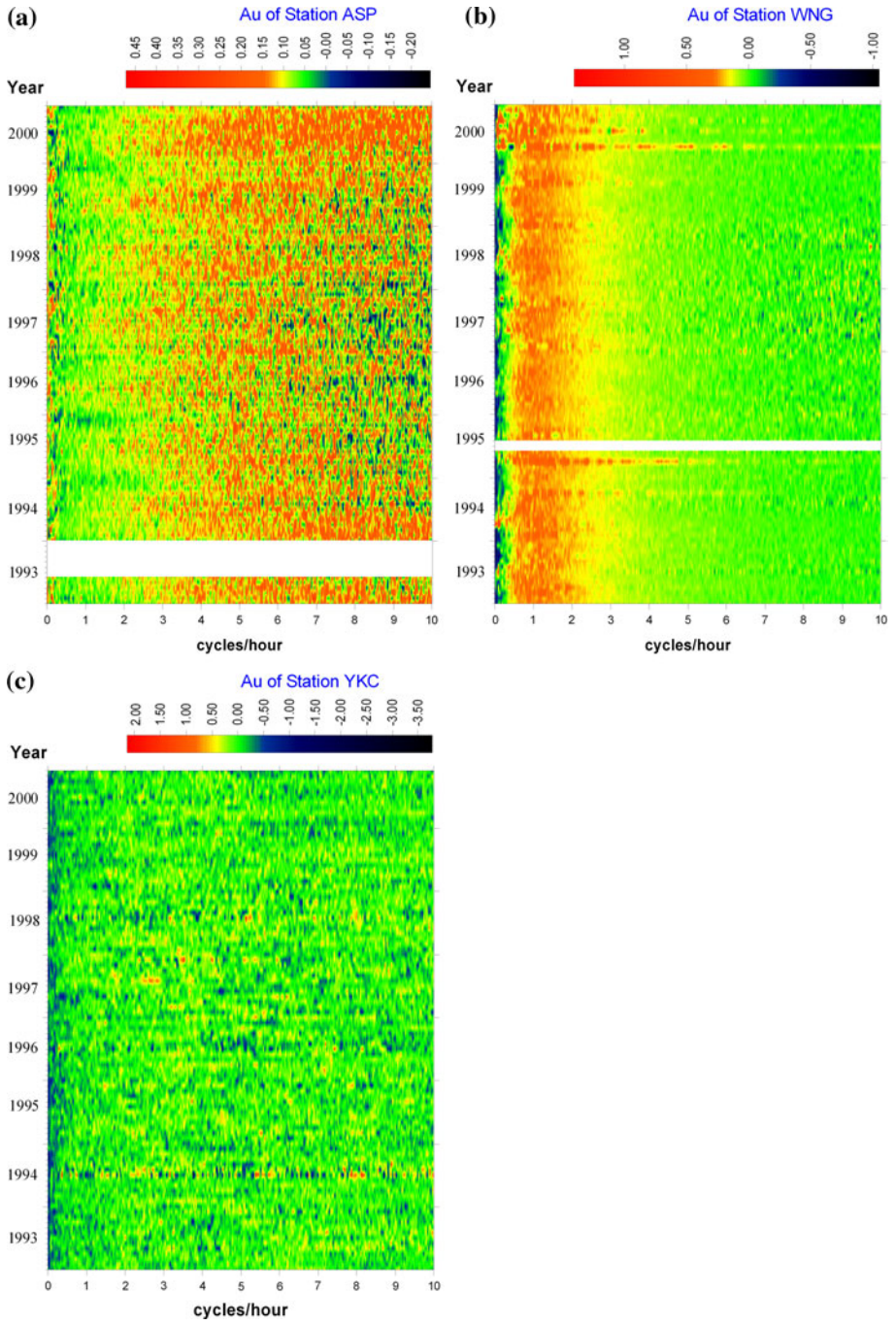

Fig. 3 Transfer functions (*Au*) calculated for frequency range between 0.1 and 10 cycles/hour from stations **a** ASP, **b** WNG and, **c** YKC during the period 1993–2000

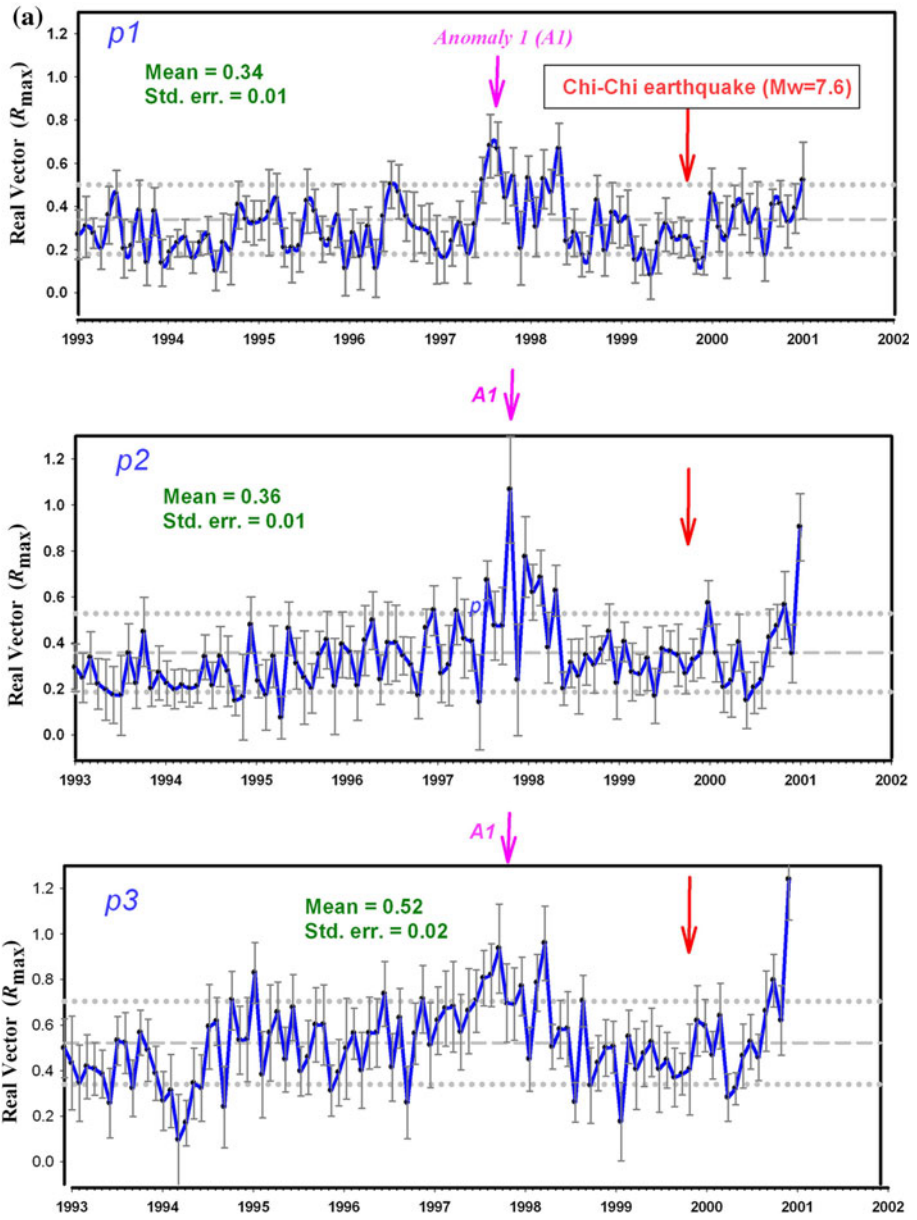

Fig. 4 Monthly averages of **a** real induction *arrow* (R_{max}) and **b** imaginary induction *arrow* (R_{min}) of induction *arrows* for period range at *P1, P2,* and *P3*. The *dashed line* denotes the mean of the whole study period, and *dotted lines* denote one standard deviation. The anomaly A1 occurs about 24 months prior the 1999 Chi-Chi earthquake

components to their single components. Since almost all spectra at Lunping reveal that there are three relatively significant periods at 24, 12, and 8 h (as Fig. 7 shows). We applied the CD method (following the method derived by Chen et al. (2007) to calculate

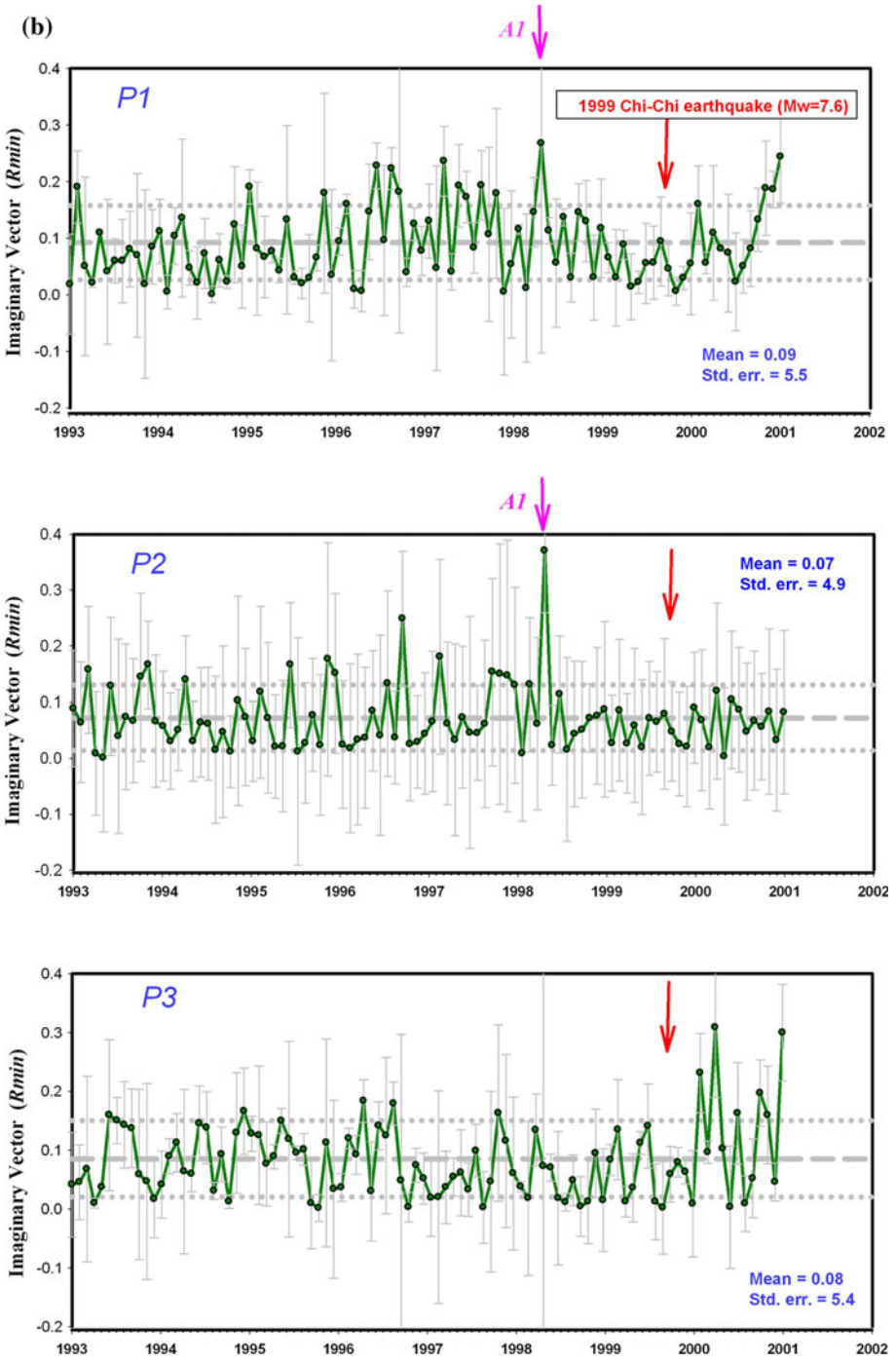

Fig. 4 continued

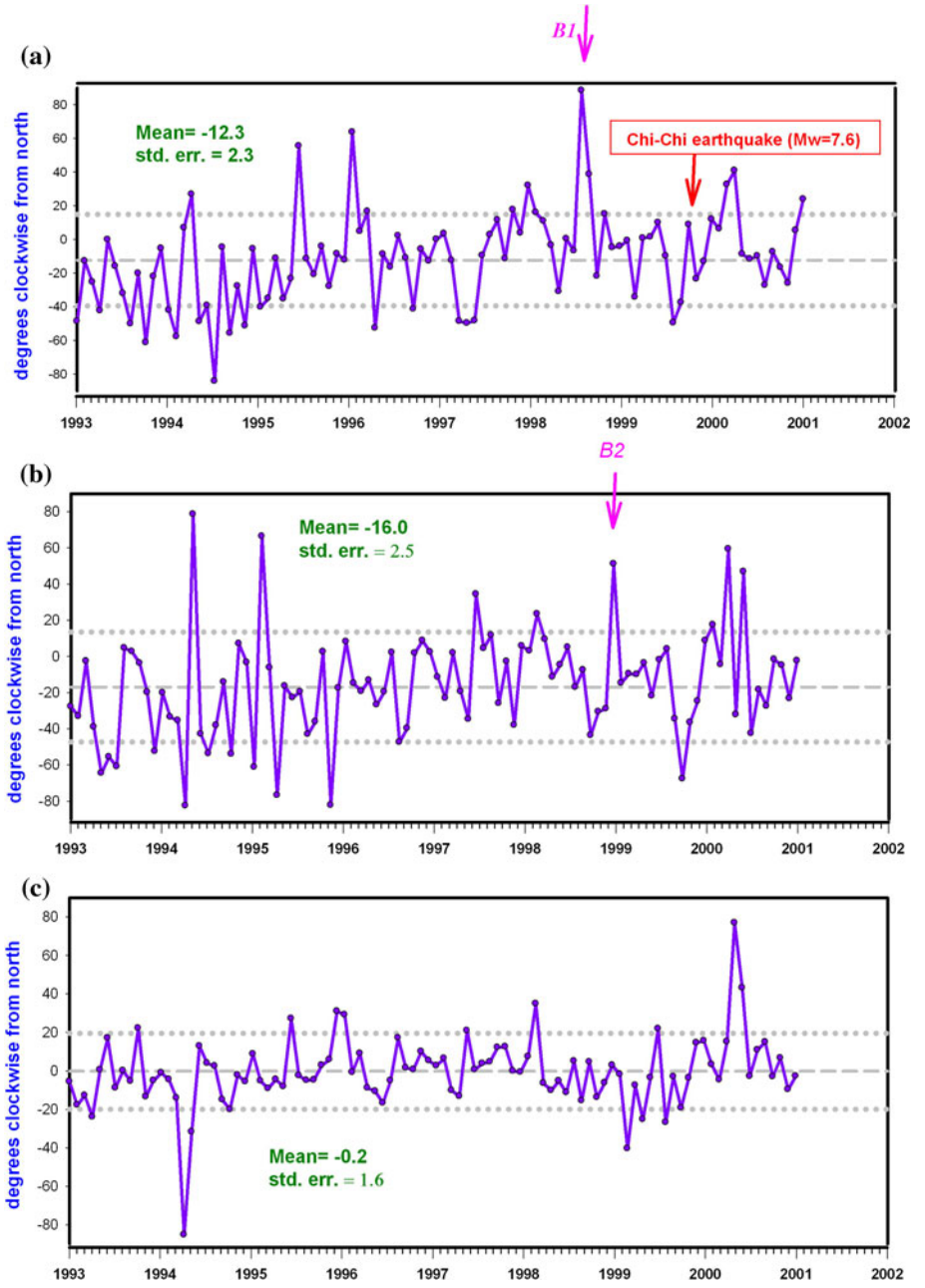

Fig. 5 Monthly average of the direction of real induction arrow at *P1*, *P2*, and *P3*, for the Lunping Observatory. The *dashed line* denotes the mean of the whole period, and *dotted lines* denote one standard deviation. The hump B1 and B2 occur about 15 months prior the 1999 Chi-Chi earthquake

three modulus of period at 24, 12, and 8 h using total intensity data. Figure 8 shows that the modulus of 12 and 8 h relative to 24 h revealing a period of 1 year. The dotted line represents the mean of each curve. It can be seen that each of the temporal variation of the

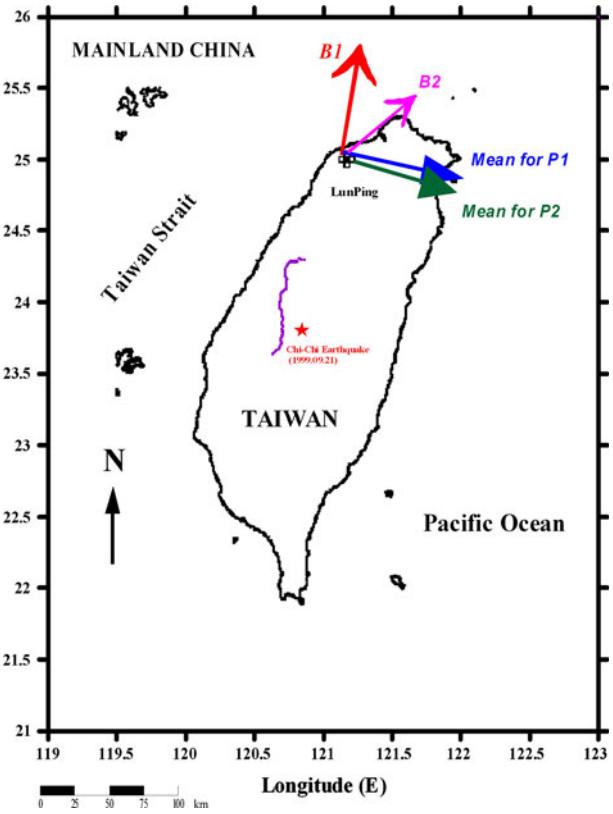

Fig. 6 The rotation of the real induction *arrows* for *P1* (*B1* in Fig. 4; denoted by *red arrow*) and *P2* (*B2* in Fig. 4; denoted by *pink arrow*)

modulus oscillated along the mean annually during the length of the study period showing very clearly the effects of an annual or semi-annual modulation. This period represents the seasonal effect. Importantly, before the 1999 Chi-Chi earthquake, the ratios of the modulus relative to the 24 h at period 12 and 8 h show a significant increase, with about 13 and 4 nT, and subsides to its normal (mean) level after the earthquake. The bulges near May 1999 in all figures can be found which are 4–5 months prior the 1999 Chi-Chi earthquake. Since the standard deviations of these two periods are 0.7746 and 0.5049, respectively, the variation amounts above are larger than two standard deviations. We considered that these variations occur locally and may be related to the 1999 Chi-Chi earthquake occurrence. However, after the earthquake, the variation subsides to its normal (mean) level. Figure 8c shows that these temporal variations of the total effect of modulus of these three characteristic periods are observed at the Lunping Observatory revealing remarkably anomalous variation before the 1999 Chi-Chi earthquake and subsides to its mean level after the large earthquake. The trend of recovery occurs after the earthquake. The other anomaly occurs in 1996 can also be found in Fig. 8. Examining the seismicities of the Taiwan area (Fig. 7 in Chen et al. 2006), we can find there is a peak value in May 1997 which is 12 months after the 1996 magnetic bulge.

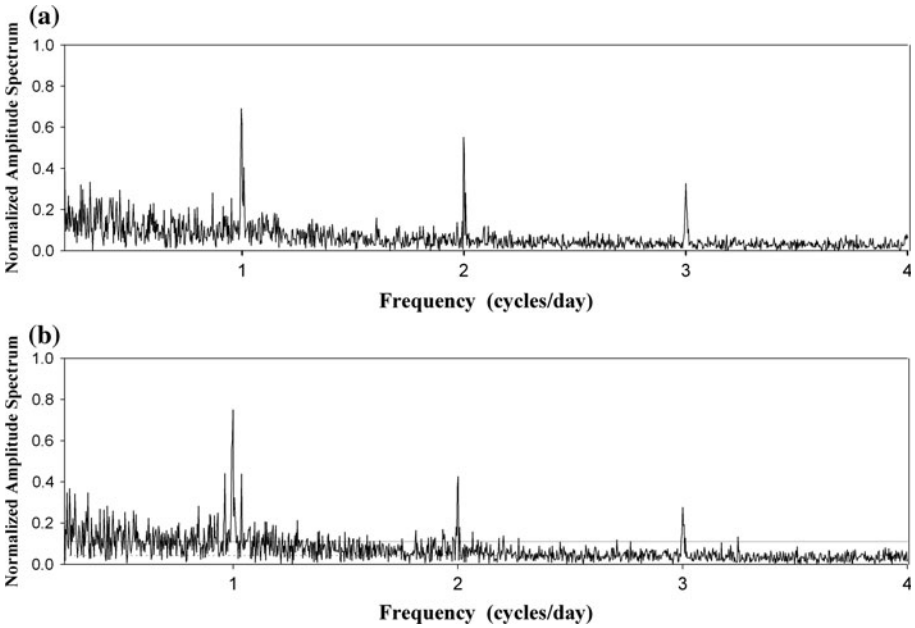

Fig. 7 Amplitude spectra of geomagnetic total intensity data at Lunping of the year **a**1999 and **b** 1994

Checking the global geomagnetic activity index (*Kp*), acquired from the National Geophysical Data Center (NGDC) for the study period, we can easily find that there is no significant variation of *Kp* within the study period (Fig. 9). It can be concluded that the variation at Lunping is a local effect rather than a global effect.

4 Discussion and conclusion

It is difficult to give an accurate quantitative explanation for the different characteristics between the real and the imaginary induction arrows especially in light of the fact that we have only the results obtained from one observatory. Roughly speaking, the magnitude and the direction of the induction arrows at Lunping may be dependent on the presence of sea water surrounding Taiwan Island and the temporal variation of a possibly extant conductivity anomaly, which is buried deeply, and associated with the earthquake preparation zone. Derived from magnitude deviation, Chen et al. (2003) found that the seismic attenuation structures *(Qs)* in the close vicinity of the focal region of the Chi-Chi earthquake increased during 1 day to 4 months following the main shock and decreased to its normal value. They suggested that the rock mechanics subsurface the earthquake preparation zone may be changed before the main shock. It also caused the conductivity changes under that area before and after the main earthquake.

Since the seasonal variation is small (Chen et al. 2006), sea temperature changes slowly with a period longer than that of our study, we consider that the conductivity of sea water should be unchanged in time during the studied period. The coast effect in the Taiwan area is minor and can be discounted (Yeh et al. 1981; Chen 1981a, b). The fact that the real induction arrow rotated gradually outwards from the earthquakes region before the earthquake occurrence, and the imaginary arrow remained unchanged can be qualitatively

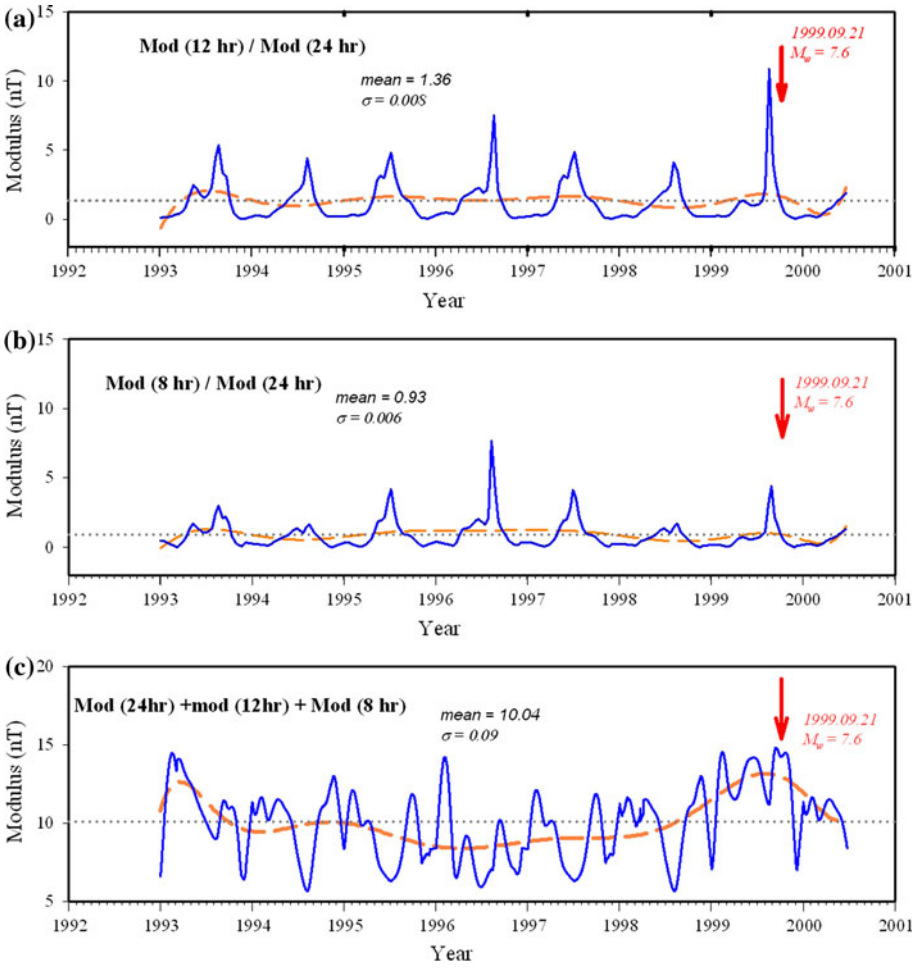

Fig. 8 Ratios of modulus of **a** period = 12 and **b** period = 8 h relative to period = 24 h. **c** Summation of the modulous of 24, 12, and 8 h for the Lunping Observatory during the interval of 1993–2000. The dotted lines represent the mean, and long-dash lines denote its linear regressions. The *arrow* represents the 1999 Chi-Chi earthquake occurrence. The humps near May 1999 in all figures can be found which are 4–5 months prior the 1999 Chi-Chi earthquake

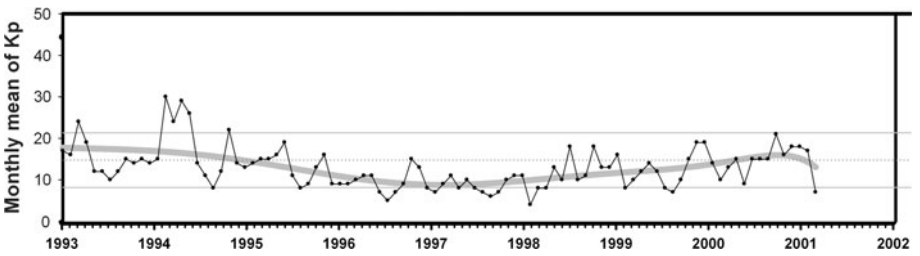

Fig. 9 The global geomagnetic activity index (*Kp*) (acquired from the National Geophysical Data Center (NGDC) during 1993–2001

explained by the elevation of the top level of the conductivity anomaly in the southern region of the Lunping Observatory. Since the temperature structure near the upper boundary is usually very complicated, we assume that the vertical gradient of temperature there might change in accordance with the movement of the subducting plate. Hence, the volume variation of highly conductivity anomaly, due to the elevation or subsidence of isogeotherm, might be related to the seismicity.

In practice, no matter which type of observation technique is being used, the source field effect should be taken into consideration. To check the influence of the source fields on the transfer functions is certainly necessary. Many calculations relevant to such a relationship using a 3-D model have been developed by Everett and Hyndman (1967), Williamson et al. (1974), Honkura (1979), Liley and Arora (1982), Chen and Fung (1985, 1986, 1989, 1993). Several models with different dimensions and conductivity have been set to calculate its theoretic values of the induction arrows and total intensity. The model with a minimum deviation between its theoretic values and the observed arrows at LNP (real induction arrow, imaginary induction arrow, and induction arrow) is set to be the optimum final one. The final model shows that the size of the anomaly body is $30 \times 40 \times 30$ km^3, and the depth of the top surface is 5 km. The conductivity of the anomaly is 0.06 S/m, and the conductivity of the host medium is 0.002 S/m. In order to investigate the source field effect on the induction arrow, we have designed a very simple 3-D model (see Fig. 10). A grid mesh of $30 \times 40 \times 30$ points is used in our calculation. The numerical results of the induction arrows calculated from the model are shown in Figs. 11 and 12. Figure 11 shows the distribution of the real induction arrows, whose components are A_u and B_u. The observed arrow in LNP has also been drawn (shown in red arrow) to compare with its calculated arrow. Figure 12 shows distribution of the calculated imaginary induction arrows and observed arrow in LNP, whose components are A_v and B_v. The numerical result of these two arrows obtained in the Lunping station shows very identical to that of the observed arrows shown in Fig. 4. We then can propose that the anomalies (*A1*), shown in Fig. 4, prior the Chi-Chi earthquake might be ascribed to the anomaly body shown in Fig. 10 which is located under the epicenter area of the Chi-Chi earthquake. Furthermore, the induction directions calculated from the model shown in Fig. 10 are shown in Fig. 13. We also find that the direction (89°) is nearly equal to the anomalies (B1 and B2) shown in Fig. 5.

As of this writing, no finding has demonstrated which periods of transfer function are meaningful for analysis. Chen and Fung (1993) analyzed the transfer functions at four

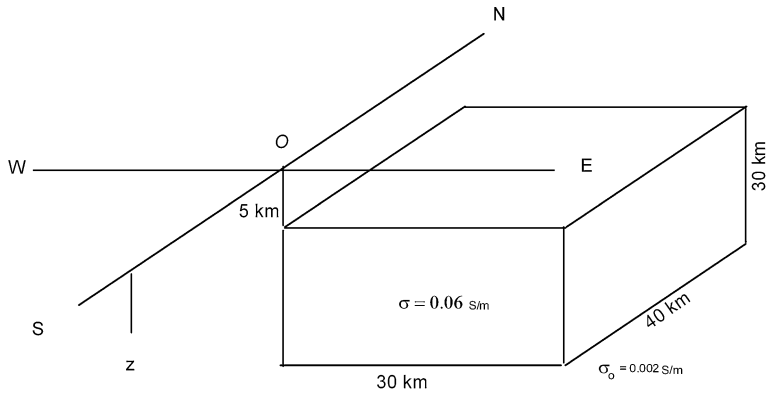

Fig. 10 Three-dimensional model of the anomaly structure

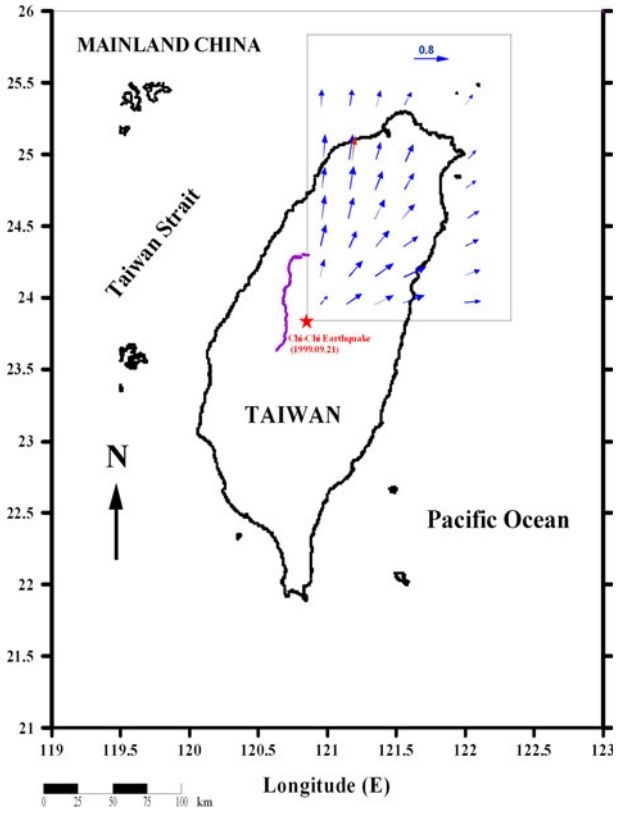

Fig. 11 Distribution of the real induction arrows (*in blue*) for the model described in Fig. 10. The observed real induction *arrow* in LNP is shown in *red arrow*

periods in 31, 25, 21, and 14 min and found some precursors before great earthquake without mentioning the criterions of why they chose these four particular periods. Chen et al. (2006)found some correlation between time change in transfer functions and seismic energy release at four periods in 30, 20, 15, and 10 min. A similar analysis of transfer functions at period of 30 min done by Shiraki (1980) also shows no discussion about how to decide upon the period. However, in this study, the transfer functions at three sensitive period ranges (*P1*, *P2*, and *P3)* can be more easily found (Fig. 2). These three sensitive periods are more probably due to some electrical conductivity anomalies. Fujiwara and Toh (1996) found that the sensitive frequency range of a transfer function is correlated with the depth of the conductivity anomaly. A shallow conductivity anomaly always causes higher frequency range. They also found that the ocean effects are almost larger than 32 min. In our study, the sensitive periods are all smaller than 32 min and indicate that the variations of the magnetic vector are caused by some shallow conductivity anomaly, not by the ocean effect.

The average annual change rate in transfer functions seems to be closely related to the preparation process of a strong earthquake. For example, the annual change rate of A for the period greater than 6 min for the Kakioka Observatory is about 0.01 before the 1923 Kanto earthquake (Yanagihara 1972). In addition, the annual changes rates of the 10-min period *Au* from the Matsuzaki and Omaezaki observatories decreased remarkably

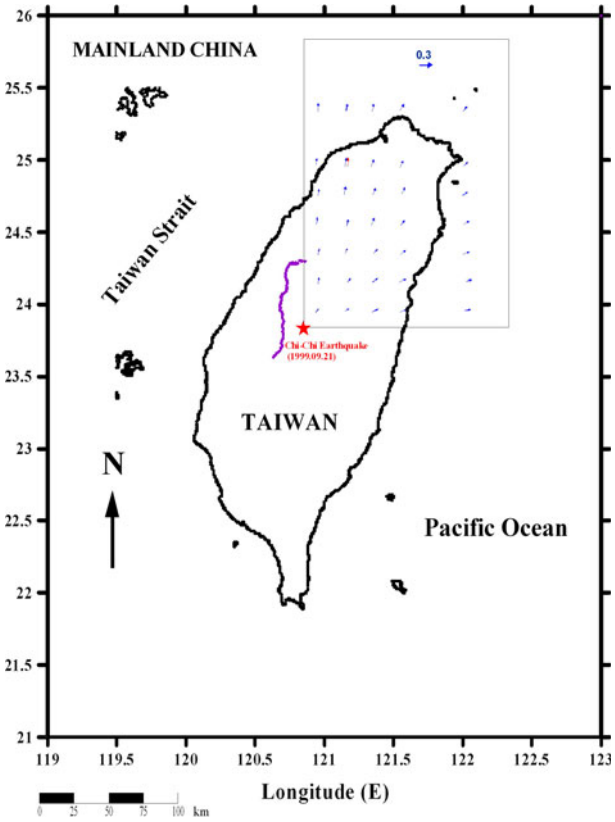

Fig. 12 Distribution of the imaginary induction arrows (*in blue*) for the model described in Fig. 10. The observed imaginary induction *arrow* in LNP is shown in *red arrow*

(up to 0.02) before a large earthquake which occurred in the Tokai area (Fujita 1990). In this study, the two abrupt changes of the real induction arrow ($R_{\max}$) and the imaginary arrow ($R_{\min}$) (*A1* in Fig. 4) are about 0.6–0.8 which are twice or triple its standard deviations. The two anomalies in direction of real induction arrow (θ_m) are all greater than 2 standard deviations more than their statistical mean, and as such it can be inferred that the anomalies are reliable.

The global geomagnetic activity index (*Kp*) (acquired from the National Geophysical Data Center (NGDC)) for the study period is plotted in Fig. 9, demonstrating that there is no significant change before the Chi-Chi earthquake. For comparison, we introduce the temporal variation in transfer functions observed at the "seismically quiet" area of the ASP and WNG observatories. We find that the temporal variation of $R_{\max}$ and $R_{\min}$ did not show the same increase in the same interval in these stations as Lunping station demonstrating that the changes of the real induction arrow ($R_{\max}$) and the imaginary arrow ($R_{\min}$) in Fig. 4 are a local effect rather than a global effect.

A universal precursor time is still a mystery. We do not have any idea about how long a precursor time should be. In our study, only one event is found with two different methods. We can hardly suggest the relationship or regulation that the precursor time should follow. More data and analyses would be helpful in resolving this problem. Further, it is difficult to give a quantitative explanation for the different characteristics between real and imaginary

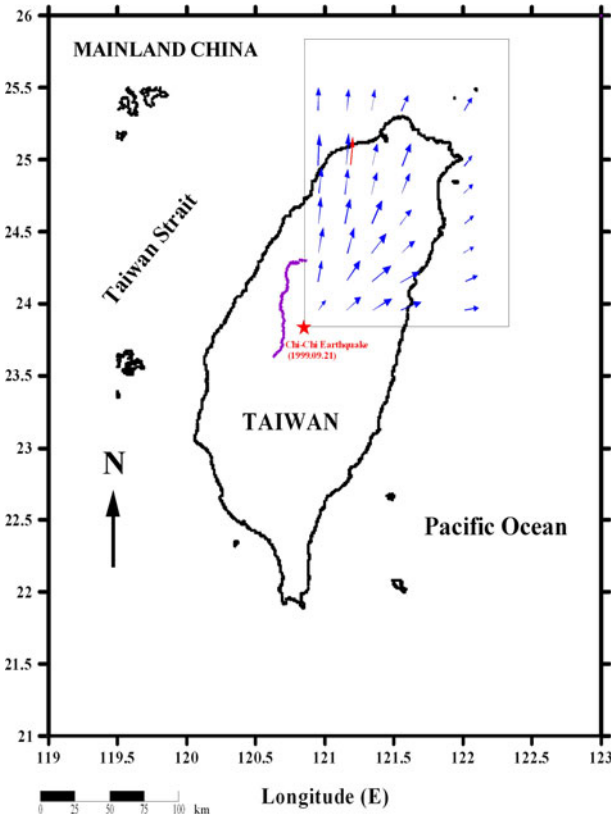

Fig. 13 Distribution of the direction of induction arrows (*in blue*) for the model described in Fig. 10. The observed induction *arrow* in LNP is shown in *red arrow*

induction arrows at the present stage of study due to the limited results obtained from the Lunping Observatory. Roughly speaking, the magnitude and direction of the real induction arrow at Lunping may be dependent on the presence of sea water surrounding Taiwan Island, and the temporal variation of a possible extant conductivity anomaly, which is buried deeply and associated with the earthquake preparation zone. We consider that the conductivity of sea water should be unchanged in the time during the studied period. The fact that the real induction arrow rotated gradually outwards from the earthquake region before the earthquake occurrence, and the imaginary arrow remained unchanged and can be qualitatively explained by the elevation of the level of the conductivity anomaly in the southern region of the Lunping Observatory, i.e., in the source region of the 1999 Chi-Chi earthquake. Figure 1 shows the epicenters of the major shock and aftershocks located south of the Lunping Magnetic Observatory and indicates that these earthquakes might be triggered by conductivity anomalies near the epicenter's area.

Finally, the transfer function estimates are averaged over 1-month intervals so that only fairly long-term precursory effects can be detected. In the Taiwan area, earthquakes occur so frequently and estimates based upon a 1-month interval are quite inappropriate to discover a single relationship between transfer function change and a single earthquake occurrence.

Acknowledgments The authors thank for many useful suggestions from Prof. C. S. Wang to improve the manuscript. The authors are greatly indebted to Mr. Yung-Po Lee, for providing geomagnetic data of the Lunping Geomagnetic Observatory. The authors also wish to thank the staff of World Data Center A for continuously providing many digital magnetograms of the Alice Spring, Wingst (WNG), and Yellow Knife (YKC) observatories during the past several years. This work was supported by the National Sciences Council, ROC under the Grants NSC-92-2119-M-003-001 and NSC-93-2119-M-003-001.

References

Banks RJ (1975) Complex demodulation of geomagnetic data and the estimation of transfer function. Geophys J R Astr Soc 43:87–101

Beamish D (1982) A geomagnetic precursory to 1979 Carlisle earthquake. Geophys J R Astr Soc 68:531–543

Chang CH, Wu YM, Shin TC, Wang CY (2000) Relocation of the 1999 Chi-Chi earthquake in Taiwan. Terr Atm Oceanic Sci 11:581–590

Chen KJ (1981a) Magnetic coast effect in northern Taiwan. Master Dissertation. National Taiwan University

Chen PF (1981b) A search for correlation between time change in transfer functions and seismic activity in north Taiwan. J Geomag Geoelectr 33:635–643

Chen CC, Chen CS (1998) Preliminary results of magnetotelluric soundings in the fold-thrust belt of Taiwan and possible detection of dehydration. Tectonophysics 292:101–117

Chen PF, Fung PCW (1985) Significance of the sign changing of the imaginary arrows in geomagnetic induction investigation. Geophys J R astr Soc 80:257–263

Chen PF, Fung PCW (1986) The frequency response of two-dimensional induction anomalies revisited. J Geomag Geolectr 38:873–881

Chen PF, Fung PCW (1989) A numerical study of some horizontal source field effects on the transfer functions and amplitude ratios in geomagnetic induction investigation. ACTA Seismological Sinica 2:274–288

Chen PF, Fung PCW (1990) Time changes in complex transfer functions at Lunping and the 1986 earthquake ($M_S = 7.6$) near Hualian. In: Organizing Committee of Conference (ed) Proceedings of the international symposium on geomagnetism. Seismological Bureau of Shanghai, China, pp 81–85

Chen PF, Fung PCW (1993) Time changes in geomagnetic transfer functions at Lunping before and after the 1986 Hualian earthquake ($M_S = 7.6$). J Geomag Geoelectr 45:251–259

Chen KJ, Wang CM, Hsu SK, Liang WT (2001) Geomagnetic basement relief of the northern Taiwan area. Terr Atm Oceanic Sci 12:441–460

Chen KJ, Chao K, Tseng YT, Lin CH, Chang CH (2003) Temporal change of Qs-1 in the 1999 Chi-Chi earthquake fault area, Taiwan. Terr Atm Oceanic Sci 14:145–158

Chen KJ, Chiu B, Lin CH (2006) A search for a correlation between time change in transfer functions and seismic energy release in northern Taiwan. Earth Planets Space 58:981–991

Chen KJ, Ho YR, Chiu B, Wang JS, Sun R, Lin CH (2007) Correlation between time change in modulus of short period geomagnetic variation and seismicity in Taiwan. Terr Atm Oceanic Sci 18:577–591

Everett JE, Hyndman RD (1967) Geomagnetic variations and electrical conductivity structure in southwestern Australia. Phys Earth Planet Int 1:24–34

Fraser-Smith AC, Bernardi A, McGill PR, Ladd ME, Helliwell RA, Villard OG Jr (1990) Low-frequency magnetic field measurements near the epicenter of the Ms 7.1 Loma Prieta earthquake. Geophys Res Lett 17:1465–1468

Fujinawa Y, Takanashi K (1994) Anomalous VLF subsurface electric field changes preceding earthquakes. Tech Note Natl Res Inst Earth Sci Disast Prev 166:61–75

Fujita S (1990) Monitoring of time changes of conductivity anomaly transfer functions at Japanese magnetic observatory network. Mem Kakioka Mag Obs 23:53–87

Fujiwara S, Toh H (1996) Geomagnetic transfer functions in Japan obtained by first order geomagnetic survey. J Geomag Geoelectr 48:1071–1101

Gong SJ (1985) Anomalous changes in transfer functions and the 1976 Tangshan earthquake ($M_S = 7.8$). J Geomag Geoelectr 37:503–508

Honkura Y (1979) Observations of short-period geomagnetic variation at Nakaizu (2): changes in transfer functions associated with the Izu-Oshima-Kinkai earthquake of 1978. Bull Earthq Res Inst Univ Tokyo 54:477–490

Hsu SK, Liu CS, Shyu CT, Liu SY, Sibuet JC, Lallemand S, Wang C, Reed D (1998) New gravity and magnetic anomaly maps in the Taiwan-Luzon region and their preliminary interpretation. Terr Atm Oceanic Sci 9:509–532

Hsu SK, Yeh YC, Lo CL, Lin ATS, Doo WB (2008) Link between crustal magnetization and earthquakes in Taiwan. Terr Atm Oceanic Sci 19:445–450

Huang YN (1990) On the digital geomagnetic observatory at Lunping, Taiwan. Phys Earth Plant Inter 59:66–77

Liley FEM, Arora BR (1982) The sign convention for quadrature Parkinson arrows in geomagnetic induction studies. Rev Geophys Space Phys 20:513–518

Liu JY, Chen YI, Tsai YB, Chuo YJ (2000) Seismo-ionospheric signatures prior to $M \geq 6.0$ Taiwan earthquakes. Geophys Res Lett 27:3113–3116

Miyakoshi J (1975) Secular variation of Parkinson vectors in a seismically active region of Middle Asia. J Faculty Gen Edu Tottori Univ 8:209–218

Nagao T, Enomoto Y, Fujinawa Y, Hata M, Hayakawa M, Huang Q, Izutsu J, Kushida Y, Maeda K, Oike K, Uyeda S, Yoshino T (2002) Electromagnetic anomalies associated with 1995 Kobe earthquake. J Geodynamics 33:401–411

Niblett ER, Honkura Y (1980) Time-dependence of electromagnetic transfer functions and their association with tectonic activity. Geophys Surv 4:97–114

Oike K, Murakami H (1993) On the relationship between shallow earthquakes and VLF noises. Tech Note Natl Res Inst Earth Sci Disast Pre 157:221–271 (in Japanese)

Parkinson WD (1959) Directions of rapid geomagnetic fluctuations. Geophys J R Astron Soc 2:1–14

Pulinets SA (1998) Seismic activity as a source of ionospheric variability. Adv Space Res 22:903–906

Rikitake T (1966) Electromagnetism and the earth's interior. Elsevier, Amsterdam, p 308

Rikitake T (1987a) Earthquake precursors in Japan: precursor time and detectability. Tectonophysics 136:263–282

Rikitake T (1987b) Magnetic and electric signals precursory to earthquakes: an analysis of Japanese data. J Geomag Geoelectr 39:47–61

Rikitake T (1997) Nature of electromagnetic emission precursory to an earthquake. J Geomag Geoelectr 49:1153–1163

Rikitake T, Yokoyama I (1955) The anomalous behavior of geomagnetic variations of short period in Japan and its relation to the subterranean structure. The 6th report. (The results of further observations and some considerations concerning the influences of the sea on geomagnetic variations). Bull Earthq Res Inst Univ Tokyo 33:297–331

Sano Y (1980) Time changes of transfer functions at Kakioka related to earthquake occurrences (I). Mem Kakioka Mag Obs 39(2):1–25

Shin TC (2000) Some seismological aspects of the Chi-Chi earthquake in Taiwan. Terr Atm Oceanic Sci 11:555–566

Shiraki M (1980) Monitoring of the time change in transfer functions in the central Japan conductivity anomaly. J Geomag Geoelectr 32:637–648

Williamson K, Hewlett C, Tammemagi HY (1974) Computer modeling of electrical conductivity structures. Geophys J R astr Soc 37:533–536

Xu WY, Qi K, Wang SM (1978) On the short period geomagnetic variation anomaly of eastern Kansu province. Acta Geophys Sinica 21:218–224 (Chinese with English abstract)

Yanagihara K (1972) Secular variation of the electrical conductivity anomaly in the central part of Japan. Mem Kakioka Mag Obs 15:1–11

Yeh YH, Tsai YB, Teng TL (1981) Investigation of geomagnetic total intensity in Taiwan from 1979 to 1981. Bull Inst Earth Sci Academia Sinica 1:157–188

Yen HY, Chen CH, Yeh YH, Liu JY, Lin CR, Tsai YB (2004) Geomagnetic fluctuations during the 1999 Chi-Chi earthquake in Taiwan. Earth Planets Space 56:39–45

Yen HY, Chen CH, Hsieh HH, Lin CR, Yeh YH, Tsai YB, Liu JY, Yu GK, Chen YR (2009) Magnetic survey of Taiwan and its preliminary interpretations. Terr Atm Oceanic Sci 20:309–314

Yoshino T, Tomizawa I, Sugimoto T (1993) Results of statistical analysis of low-frequency seismogenic EM emissions as precursories to earthquakes and volcanic eruptions. Phys Earth Planet Inter 77:21–31

Zeng X, Lin Y, Xu C, Yang SO (2001) Turning changes in evolution of geomagnetic field and infrastructural analysis of earthquake prediction. Kybernets Int J Sys Cybernet 30:365–377

Zeng X, Hayakawa M, Lin Y, Xu C (2002) Infrastructrual analysis of geomagnetic field and earthquake prediction. In: Hayakawa M, Molchannov OA (eds) Seismo electromagnetics: lithosphere-atmosphere-ionosphere coupling. TERRAPUB, Tokyo, pp 463–468